Substituent Effects in the Iron 2p and Carbon 1s Edge Near-Edge X-ray Absorption Fine Structure (NEXAFS) Spectroscopy of Ferrocene Compounds

E. Otero,[†] R. G. Wilks,[‡] T. Regier,[‡,§] R. I. R. Blyth,[§] A. Moewes,[‡] and S. G. Urquhart*[,†,#]

Department of Chemistry, University of Saskatchewan, 110 Science Place, Saskatoon, Saskatchewan S7N 5C9, Canada, Department of Physics and Engineering Physics, University of Saskatchewan, 116 Science Place, Saskatoon, Saskatchewan S7N 5C9, Canada, and Canadian Light Source, University of Saskatchewan, 101 Perimeter Road, Saskatoon, Saskatchewan S7N 0X4, Canada

Received: June 14, 2007; In Final Form: October 27, 2007

The iron 2p and carbon 1s near-edge X-ray absorption fine structure (NEXAFS) spectra of substituted ferrocene compounds ($Fe(Cp-(CH_3)_5)_2$, $Fe(Cp)(Cp-COOH)$, $Fe(Cp-COOH)_2$, and $Fe(Cp-COCH_3)_2$) are reported and are interpreted with the aid of extended Hückel molecular orbital (EHMO) theory and density functional theory (DFT). Significant substituent effects are observed in both the Fe 2p and C 1s NEXAFS spectra. These effects can be related to the electron donating/withdrawing properties of the cyclopentadienyl ligands and their substituents as well as the presence of π^* conjugation between the cyclopentadienyl ligand and unsaturated substituents.

1. Introduction

Ferrocene-functionalized materials are finding a wide application in polymer, molecular electronics, and bioorganometallic materials.[1−6] For example, the use of transition metal species in the polymer backbone or side chain is useful for optimizing polymer solubility, as well as the material's electric, magnetic, optical, redox, and mechanic properties.[7] With the development of new synthetic routes, ferrocene-based polymers and macromolecules are being increasingly examined.[8−10] Recent studies show potential applications as photonic devices, variable refractive-index materials, magnetic and semiconducting nanomaterials, composite materials, ceramic and coating agents, to name a few.[11−13] The unusual electronic properties of ferrocene are of interest in bioorganometallic chemistry,[1] where materials based on the ferrocene-functionalization of amino acid/peptide materials or nucleic acids/DNA are being used to create biomaterials and biosensors,[2] and where ferrocene conjugates of drug-carrier polymers show promising results in cancer chemotherapy research.[14]

Near-edge X-ray absorption fine structure (NEXAFS) spectroscopy is a synchrotron based technique frequently used to investigate the chemical, electronic and structural properties of organic and inorganic materials.[15,16] Recently, NEXAFS spectroscopy has been used to examine organoiron species such as ferrocene functionalized self-assembled monolayers,[6] peptides,[17,18] polymers,[19] and iron sites in biological molecules.[20] Our research groups are interested in the characterization of organoiron species by NEXAFS spectroscopy, for the examination of ferrocene modified peptide materials (AM and RW)[17,18] or to characterize functionalized organoiron polymers (SGU and EO).[21,22] Of general interest is the use of NEXAFS spectroscopy to explore "substituent effects", that is, the sensitivity of NEXAFS spectroscopy to functionalization of the Cp-ring in ferrocene molecules.

Bis(η^5-cyclopentadienyl)iron or ferrocene was synthesized for the first time in 1951 and its unique structure elucidated only 1 year after.[23,24] Ferrocene [$Fe(C_5H_5)_2$] is a neutral molecule containing an iron atom in a +2 oxidation state, sandwiched between two cyclopentadiene (Cp) rings, each bearing a negative charge. The two Cp rings are approximately 3.32 Å from each other and are observed in eclipsed (D_{5h}) and staggered (D_{5d}) conformations.[25] The central metal atom is equivalently bound to all 10 carbon atoms via covalent bonding interactions. The ligand field generated by the two Cp rings is sufficiently greater than the spin pairing energy; as a result ferrocene is a d^6 low-spin diamagnetic compound with closed shell electron configuration, $(e_{2g})^4$ $(a_{1g})^2$ in the D_{5d} conformation.

Ferrocene and related species have been investigated by NEXAFS spectroscopy or inner shell electron energy loss spectroscopy (ISEELS) at the Fe 1s, 2p, and 3p edges and at the C 1s edge.[26−31] We will use NEXAFS as a generic label to refer to the results of NEXAFS and ISEELS spectroscopy, except where specificity is necessary. The NEXAFS spectra of transition metal compounds are subject to competing models of atomic multiplet theory[32] and covalent bonding models such as molecular orbital theory.[20,33,34] We have recently studied the NEXAFS spectroscopy of ferrocene (Fe^{2+}) and ferrocenium (Fe^{3+}) species and found that the covalent bonding model is effective at interpreting the NEXAFS spectra of closed shell ferrocene, but that multiplet effects dominate the spectrum of open shell ferrocenium.[35] Previous studies on nickel and copper complexes have indicated similar contributions from covalent hybridization between metal 3d and ligand orbitals to Ni 2p and Cu 2p NEXAFS spectra.[36−39]

Early experimental and theoretical NEXAFS or ISEELS studies on metallocenes and carbonyl complexes showed that the metal 2p NEXAFS spectra were sensitive to the identity of the ligand, less so to chemical substitution on the ligand, and insensitive to molecular symmetry.[28−30,40] Former study on alkane and alkene substituted ferrocene complexes showed that

* Corresponding author. E-mail: stephen.urquhart@usask.ca.
[†] Department of Chemistry.
[‡] Department of Physics and Engineering Physics.
[§] Canadian Light Source.
[#] Contribution prepared while on sabbatical leave at the Canadian Light Source.

10.1021/jp074625w CCC: $40.75
Published on Web 01/09/2008

SCHEME 1: Chemical Structures Examined in This Paper

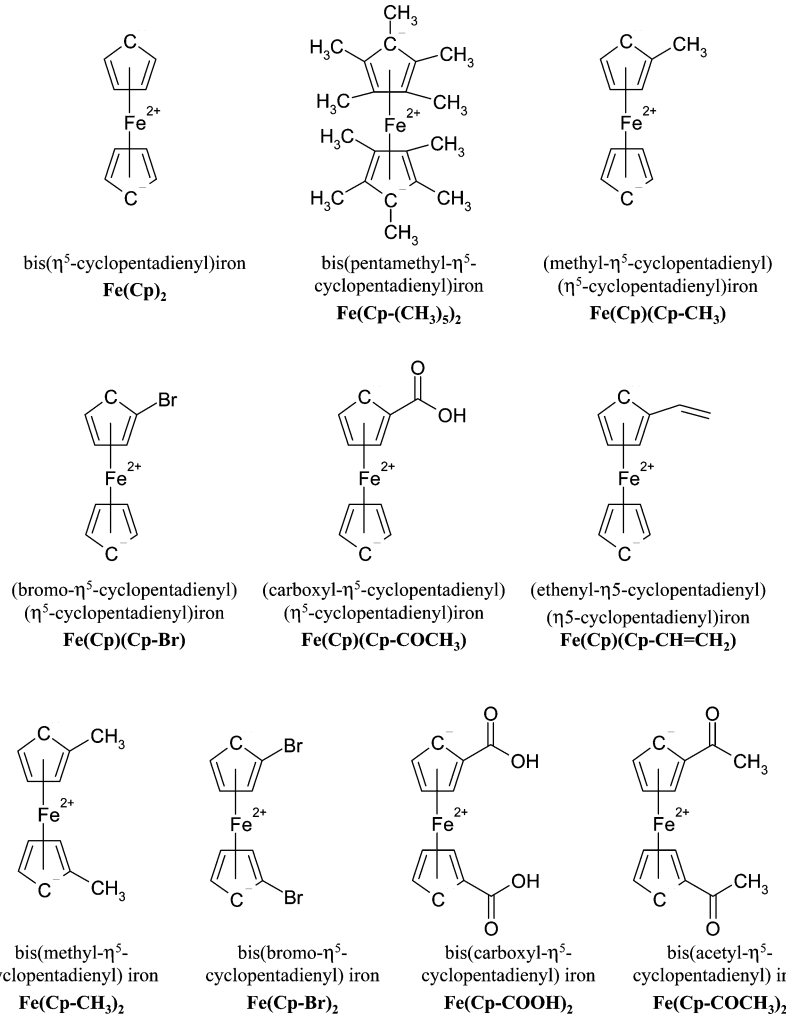

ISEELS of metallocenes had at Fe 2p edge limited sensitivity to chemical substitution at remote locations on the cyclopentadiene ligand.[29] With the higher energy resolution routinely available with modern synchrotron beamlines (<0.1 eV, in contrast to the ~0.5−0.7 eV resolution of ISEELS spectroscopy), significant new chemical insight is attained in the NEXAFS spectra of substituted ferrocene derivatives.

In this work, we explore the strength and origin of substituent effects in the NEXAFS spectra of substituted ferrocene molecules. We have acquired Fe 2p and C 1s NEXAFS spectra of a wide range of substituted ferrocene species, and used extended Hückel molecular orbital (EHMO) and density functional theory (DFT) theory calculations to help assign these NEXAFS spectra.

2. Experimental Section

2.1. Reagents and Sample Preparation. The following compounds were obtained commercially from Aldrich and used without further purification: bis(pentamethyl-η^5-cyclopentadienyl)iron (or decamethylferrocene, $Fe(Cp-(CH_3)_5)_2$, 97%), bis(carboxyl-η^5-cyclopentadienyl)iron (or 1,1′-ferrocenedicarboxylic acid, $Fe(Cp-COOH)_2$, 96%), bis(acetyl-η^5-cyclopentadienyl)iron (or 1,1′-diacetylferrocene, $Fe(Cp-COCH_3)_2$, 96%), and iron(III) oxide (Fe_2O_3, 99%). (Carboxyl-η^5-cyclopentadienyl)(η^5-cyclopentadienyl)iron (or ferrocenecarboxylic acid Fe(Cp)(Cp−COOH), 97%) was purchased from Strem Chemicals and potassium hexacyanoferrate(II) and potassium hexacyanoferrate(III) were purchased from BDH ($K_4[Fe(CN)_6]$ 99% and $K_3[Fe(CN)_6]$ 99%) and used as received. Sulfur hexafluoride (SF_6, 99%) was obtained from air liquid Canada. The molecular structures of the solid-phase reagents are presented in Scheme 1.

Solid samples were prepared by pressing milligram amounts of each compound into indium foil (0.25 mm thick, 99.99% purity, Aldrich) immediately before insertion in the measurement chamber.

Gold sample used in the normalization process were prepared by first depositing 20 Å of Chromium (chromium plated tungsten rod; R.D. Mathis), followed by ~100 Å of gold on clean silicon wafer (N-type, P doped, orientation (100), 1−10 Ω/cm resistivity; Silicon Inc.), using a thermal thin film deposition system (Datacomp Scientific).

2.2. NEXAFS Measurements. The NEXAFS spectra were obtained by recording the sample current in total electron yield (TEY) mode using the spherical grating monochromator (SGM) on beamline 11-ID.1 at the Canadian Light Source (University of Saskatchewan, Canada). This beamline is equipped with a Dragon-type spherical grating monochromator and was designed for high-resolution soft X-ray spectroscopic studies.[41] The spectroscopic resolving power ($E/\Delta E$) is estimated as better than 3200.

At Fe 2p edge the spectra were normalized using the double normalization method:

$$\text{normalized spectra} = [I/I_0]/[I_R/I_{0R}] \quad (1)$$

where I corresponds to the sample current and I_0 the current from a mesh-monitor located upstream of the sample. The reference current (I_R) was recorded from a gold coated silicon wafer.

At carbon edge all spectra were normalized by the following equation:

$$\text{normalized spectra} = [\text{sample current, } I]/[\text{gold-reference current, } I_R] \quad (2)$$

Proper normalization is critical in C 1s NEXAFS spectroscopy. Full details of the normalization processes are presented in the Supporting Information.

2.3. NEXAFS Energy Scale Calibration. Energy values reported in the literature for Fe 2p resonances are highly inconsistent[20,42−47] due to the lack of an accurate energy scale calibration method. For example, the first peak in $K_4[Fe(CN)_6]$ has been calibrated to 710.35,[42] 710.09,[45] or 709.2 eV[46] by different authors. Here, we have calibrated the energy of NEXAFS transitions in a series of model compounds to an *absolute energy scale*, provided by the F 1s NEXAFS spectrum of SF_6(g) that was previously calibrated by inner shell electron energy loss spectroscopy (ISEELS).[48] ISEELS measurements provides an accurate measurement of the energy of these transitions as the energy difference between the unscattered electron beam ("zero loss") and the inelastically scattered electrons corresponding to a specific electronic transition can be measured directly and accurately.

We have calibrated the NEXAFS energy scale for a series of solid iron compound standards by simultaneously measuring the NEXAFS spectra of gaseous SF_6 and these solid iron compounds. We have selected two low-spin complexes $K_4[Fe^{II}(CN)_6]$ and $K_3[Fe^{III}(CN)_6]$ and high-spin ionic compound Fe_2O_3 as our absolute calibration standards, to permit a direct comparison to previous experimental studies that used these molecules as relative calibration standards.[20,42−47]

The NEXAFS spectrum of SF_6 was measured in total ion yield (TIY) in a gas cell upstream from the absorption chamber. This cell is isolated by two 150 nm thick aluminum windows, and was filled with SF_6 at the beginning of the measurements. The NEXAFS spectra of the solid state standards were measured by sample current total electron yield (TEY) down stream of the gas cell, at the same time as the SF_6 TIY spectra. The presence of SF_6 in the photon beam pathway leads to series of dips in the NEXAFS spectrum of the standards, due to the reduced transmission at these energies. Figure 1a presents NEXAFS spectrum of $K_4[Fe(CN)_6]$ preceded by fluorine 1s edge absorption spectrum of SF_6. NEXAFS spectra of SF_6, $K_4[Fe(CN)_6]$, $K_3[Fe(CN)_6]$, and Fe_2O_3 are presented in Figures 1b−e; the resonance energy values reported after absolute calibration using SF_6 are listed in Table 1.[48]

The energy scale at the carbon 1s edge was calibrated relative to the C 1s NEXAFS spectrum of urea in the solid phase. In gas-phase urea it is characterized by a strong and narrow absorption peak assigned to C 1s → $\pi^*_{(C=O)}$ and reported at 289.53 eV by Urquhart et al., after an ISEELS absolute energy scale calibration.[49]

2.4. Calculations. Fe 2p NEXAFS spectra were interpreted with the aid of extended Hückel molecular orbital (EHMO) theory using the computer aided composition of atomic orbitals (CACAO) program.[50] EHMO calculations are used to explore effects of covalent bonding in these species as they are well parametrized for organoiron species and are effective for qualitatively exploring the effects of conjugation in the NEXAFS spectra of organic species.[51−53] DFT calculations are also appropriate for organoiron compounds;[18] however, our particular version of the DFT program could not perform these Fe 2p calculations at the time of this investigation.

Cartesian coordinates of $Fe(Cp)_2$, $Fe(Cp-(CH_3)_5)_2$, Fe(Cp)-(Cp−COOH), $Fe(Cp-COOH)_2$, $Fe(Cp-COCH_3)_2$, bis(methyl-

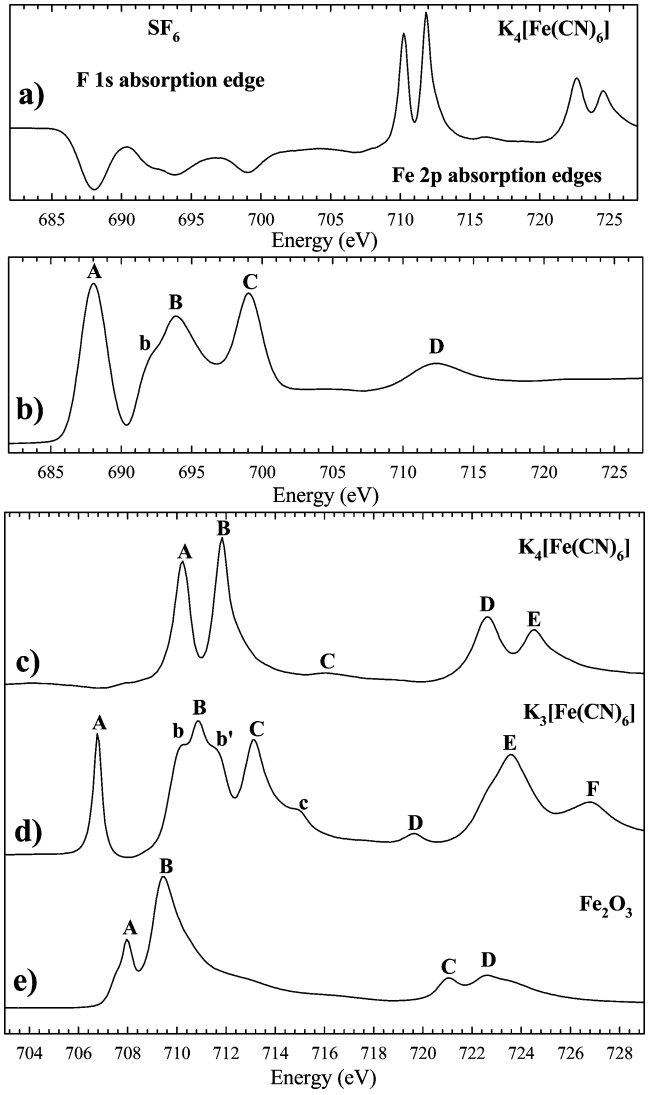

Figure 1. (a) F 1s and Fe 2p NEXAFS spectra of $K_4[Fe(CN)_6]$ with traces of SF_6 absorption. (b) F 1s NEXAFS spectrum of SF_6. (c) Fe 2p NEXAFS spectrum of $K_4[Fe(CN)_6]$, iron(II). (d) Fe 2p NEXAFS spectrum of $K_3[Fe(CN)_6]$, iron(III). (e) Fe 2p NEXAFS spectrum of Fe_2O_3.

TABLE 1: Energy (eV) of Features in the F 1s and Fe 2p NEXAFS Spectra of SF_6, $K_4[Fe(CN)_6]$, and $K_3[Fe(CN)_6]$ and Fe_2O_3

peak labels[a]	SF_6 (this study)	SF_6 (ref 48)	$K_4[Fe(CN)_6]$	$K_3[Fe(CN)_6]$	Fe_2O_3
A	688.04	688.0	710.25	706.78	707.97
b	692.40	692.4		710.27	
B	693.90	694.0	711.85	710.86	709.45
b′				711.5	
C	699.04	698.9	716	713.12	721.1
c				714.8	
D	712.2	712.1	722.7	719.6	722.6
E			724.6	721.58	
F				726.8	

[a] These labels correspond to peak identification in Figure 1. Common labels are used for convenience and do not imply a common spectroscopic assignment.

η^5-cyclopentadienyl)iron (or 1,1′-dimethylferrocene, Fe(Cp−CH_3)$_2$), and bis(bromo-η^5-cyclopentadienyl)iron (or 1,1′-dibromoferrocene, Fe(Cp−Br)$_2$) were obtained from the published X-ray crystallography parameters.[54−60] For Fe(Cp)(Cp−COOH) and Fe(Cp−$COCH_3$)$_2$ the coordinates of the hydrogen atoms were refined by geometry optimization of the molecules in the ground state using StoBe (see below) and keeping all atoms frozen except for hydrogen. The Cartesian coordinates of (methyl-η^5-cyclopentadienyl)(η^5-cyclopentadienyl)iron (or methylferrocene, Fe(Cp)(Cp−CH_3)) and (bromo-η^5-cyclopentadienyl)(η^5-cyclopentadienyl)iron (or bromoferrocene, Fe(Cp)(Cp−Br)) were estimated from the coordinates of the disubstituted molecules (Fe(Cp−CH_3)$_2$ and Fe(Cp−Br)$_2$) and refined by geometry optimization on all atoms of the molecules in the ground state. Cartesian coordinates of (vinyl-η^5-cyclopentadienyl)(η^5-cyclopentadienyl)iron (or vinylferrocene, Fe(Cp)(Cp−CH═CH_2)) were estimated from the published X-ray crystallography parameters of the biferrocene compounds and refined by a ground state geometry optimization calculation on all atoms in the molecule.[61,62]

The structures for Fe(Cp)$_2$ and Fe(Cp−$(CH_3)_5$)$_2$ have D_{5d} symmetry, and the Fe(Cp)(Cp−CH_3), Fe(Cp)(Cp−Br), Fe(Cp)-(Cp−COOH), (Fe(Cp)(Cp−CH═CH_2), Fe(Cp−COOH)$_2$, Fe-(Cp−$COCH_3$)$_2$, Fe(Cp−CH_3)$_2$, and Fe(Cp−Br)$_2$ structures are based on an eclipsed (D_{5h}) configuration.

In the EHMO calculations, the equivalent ionic core virtual orbital model (EICVOM)[63] was used to account for electronic relaxation due to the creation of the core hole. In this model, the core excited atom is replaced by the atom with one greater nuclear charge (e.g., $Z + 1$ approximation), and the molecule is given a positive charge to correct the valence electron count. The atomic propensity approximation is used to calculate the intensity of the spectroscopic features. Within the linear combination of atomic orbital−molecular orbital (LCAO−MO) description, the states accessed by the highly localized core excitation transitions are well described by the unoccupied atomic orbitals on the core excited atom. Transitions to these unoccupied atomic orbitals on the core excited atom can be described by the Laporte selection rule ($\Delta l = \pm 1$) for atomic electronic transitions (e.g., 2p → 3d; 2p → 4s), and the spectroscopic intensities are assumed to be proportional to the sum of the square of the LCAO coefficients for these atomic orbitals on the core excited atom, for each virtual MO.

Simulated spectra were obtained by calculating a Gaussian line shape for each transition using the program SIMILE2.[64] As EHMO is a valence-only method, the core binding energy is not calculated, and we present our results on an orbital energy scale (orbital energy is the negative of the term value). Line widths of 0.6 eV full width at half-maximum (fwhm) were used for transitions to states below the ionization potential. These values were selected to approximately model the experimental line width.

Ground state DFT calculations and simulated C 1s NEXAFS spectra were performed using the Stockholm-Berlin version 2.1 of deMon (StoBe2005 dated 12/9/2005).[65] This program is based on self-consistent solutions of the Kohn−Sham density functional theory (DFT). The X-ray absorption spectroscopy (XAS) calculations presented here were performed following the same procedure as in Wilks et al. study of ferrocene-labeled peptides.[18] The NEXAFS spectra are simulated by calculating the transition probabilities between half-occupied core hole and optical orbital optimized in the potential of this 0.5 occupied core hole excited molecule. For all atoms, in the ground and excited state calculations, triple-ζ plus valence polarization (TZVP) orbital basis sets were used as well as TZVP derived A5 auxiliary basis sets. For the atom from which the core excited electron originates, the iii-igol basis set has been employed. The core potential model was applied on all other carbon atoms to avoid mixing with the core excited carbon atom. NEXAFS curves were obtained by Gaussian convolution of the discrete energy values generated by StoBe. Line widths of 0.4 eV full width at half-maximum (fwhm) were used for transitions below 290 eV, 2 eV fwhm above 300 eV, and a linear increase from 0.4 to 2 eV fwhm between 290 and 300 eV. These widths are intended to approximately match experimental line widths, mimicking vibrational broadening beneath the edge and lifetime broadening above the core edge. Nonequivalent atoms were calculated separately and X-ray absorption spectra summed-up afterward. (individual spectrum of nonequivalent carbon atoms in Fe(Cp−$(CH_3)_5$)$_2$, Fe(Cp)(Cp−COOH), Fe(Cp−COOH)$_2$, and Fe(Cp−$COCH_3$)$_2$ are presented as Supporting Information, Figures S3−S6).

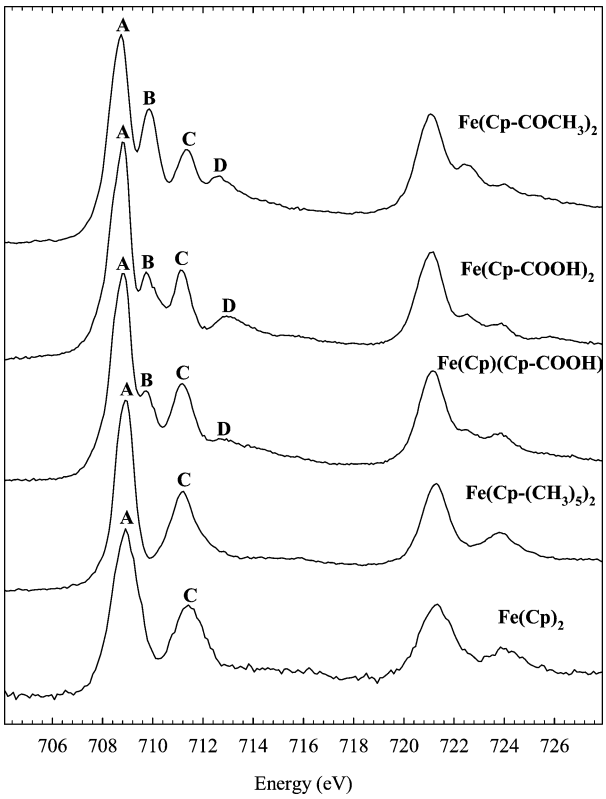

Figure 2. Fe 2p edge ISEELS spectrum of Fe(Cp)$_2$ (reproduced from ref 29) and the Fe 2p NEXAFS spectra of Fe(Cp−$(CH_3)_5$)$_2$, Fe(Cp)-(Cp−COOH), Fe(Cp−COOH)$_2$, and Fe(Cp−$COCH_3$)$_2$. The spectra have been offset by a constant for clarity.

3. Results

3.1. Fe 2p Edge. Figure 2 presents the Fe 2p ISEELS spectrum of Fe(Cp)$_2$ (reproduced from ref 29) and the Fe 2p NEXAFS spectra of the substituted ferrocene compounds Fe-(Cp−$(CH_3)_5$)$_2$, Fe(Cp)(Cp−COOH), Fe(Cp−COOH)$_2$, and Fe-(Cp−$COCH_3$)$_2$. The spectrum of Fe(Cp)$_2$ is reproduced from the literature as it is too volatile for examination at room temperature.

The transition energies and assignments for these compounds are presented in Table 2. The Fe $2p_{1/2}$ edge features resemble those observed at the Fe $2p_{3/2}$ edge; this discussion will focus on transitions at the Fe $2p_{3/2}$ edge. The Fe 2p spectra of Fe-(Cp)$_2$[28,29] and Fe(Cp−$(CH_3)_5$)$_2$ show two well resolved features

TABLE 2: Transition Energies (eV) and Assignments for the Fe 2p NEXAFS Spectra (Figure 2) of Ferrocene and Substituted Ferrocene Compounds[a]

label	$Fe(Cp)_2$ [29]	$Fe(Cp-(CH_3)_5)_2$	Fe(Cp)(Cp−COOH)	$Fe(Cp-COOH)_2$	$Fe(Cp-COCH_3)_2$	assignment
A			708.82	708.82	708.72	Fe $2p_{3/2} \rightarrow$ **Fe** $\mathbf{3d_{xz}}/\pi^*_{(Cp-COO\,H)\,(Cp-COR)}$
						Fe $2p_{3/2} \rightarrow$ **Fe** $\mathbf{3d_{yz}}/\pi^*_{(Cp)}$
A	708.9	708.87				Fe $2p_{3/2} \rightarrow$ **Fe** $\mathbf{3d_{xz,yz}}/\pi^*_{(Cp)}$
B			709.74	709.75	709.84	Fe $2p_{3/2} \rightarrow$ Fe $3d/\pi^*_{(Cp-COOH)\,(Cp-COR)}$
C	711.5	711.18	711.17	711.14	711.34	Fe $2p_{3/2} \rightarrow$ Fe $3d/\pi^*_{(Cp)}$
D			712.8	712.9	712.62	Fe $2p_{3/2} \rightarrow$ Fe $3d/\pi^*_{(Cp-COOH)\,(Cp-COR)}$
	721.2	721.27	721.50	721.11	721.08	Fe $2p_{1/2} \rightarrow$ **Fe** $\mathbf{3d_{xz}}/\pi^*_{(Cp-COO\,H)\,(Cp-COR)}$
						Fe $2p_{1/2} \rightarrow$ **Fe** $\mathbf{3d_{yz}}/\pi^*_{(Cp)}$
			722.6	722.5	722.5	Fe $2p_{1/2} \rightarrow$ Fe $3d/\pi^*_{(Cp-COOH)\,(Cp-COR)}$
	723.9	723.82	723.8	723.8	724.0	Fe $2p_{1/2} \rightarrow$ Fe $3d/\pi^*_{(Cp)}$
				725.8		Fe $2p_{1/2} \rightarrow$ **Fe** $\mathbf{3d_{xz}}/\pi^*_{(Cp-COO\,H)}$

[a] Localization of the molecular orbital on the metal or a ligand is indicted by bold script. Transition energy values for $Fe(Cp)_2$ were reproduced from ref 29.

(A and C). The Fe 2p spectra of Fe(Cp)(Cp−COOH), $Fe(Cp-COOH)_2$, and $Fe(Cp-COCH_3)_2$ show features (A and C) similar to those for $Fe(Cp-(CH_3)_5)_2$ and $Fe(Cp)_2$ but at slightly lower energy. In the Fe 2p spectra of Fe(Cp)(Cp−COOH), $Fe(Cp-COOH)_2$, and $Fe(Cp-COCH_3)_2$, two new features (B and D) are observed at ∼709.7 and 712.8 eV, respectively. For carboxylic acid substituted ferrocene compounds the intensity of these features scales approximately with the number of substituents on the Cp ring; i.e., B and D are stronger for $Fe(Cp-COOH)_2$ than for Fe(Cp)(Cp−COOH). The origin of these features will be discussed below, with the aid of EHMO calculations.

3.2. Carbon 1s Edge. The C 1s ISEELS spectrum of $Fe(Cp)_2$ (reproduced from ref 31) and the C 1s NEXAFS spectra of the substituted ferrocene compounds $Fe(Cp-(CH_3)_5)_2$, Fe(Cp)(Cp−COOH), $Fe(Cp-COOH)_2$, and $Fe(Cp-COCH_3)$ are presented in Figure 3. Transition energies and assignments are presented in Table 3.

The C 1s spectrum of $Fe(Cp-(CH_3)_5)_2$ resembles that of $Fe(Cp)_2$, with two sharp features A and C (Figure 3). An additional feature E is observed at 287.91 eV, attributed to C $1s_{(CH_3)} \rightarrow \sigma^*_{C-H}$ transitions from the methyl group. In the C 1s spectrum of Fe(Cp)(Cp−COOH), the feature A shifts ∼0.4 eV to lower energy and feature C appears at a similar energy. A new feature B is observed between A and C (at 286.3 eV) as well as a broad feature D above 288 eV. The intensity of B and D increases approximately with the number of substituents for Fe(Cp)(Cp−COOH) and $Fe(Cp-COOH)_2$. The spectrum of $Fe(Cp-COCH_3)_2$ shows a strong attenuation of the intensity of feature A. The assignment of these features will be interpreted below, with the aid of DFT calculations.

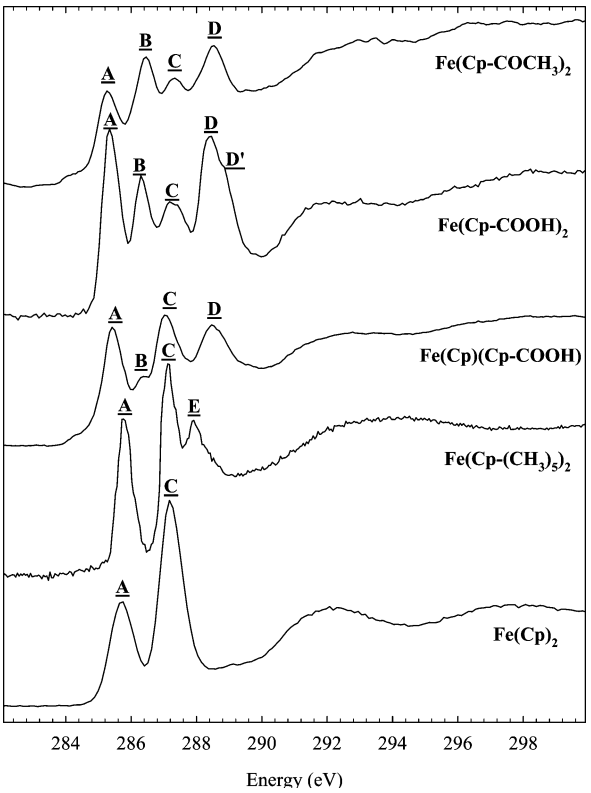

Figure 3. C 1s edge ISEELS spectrum of $Fe(Cp)_2$ (reproduced from ref 29) and the C 1s edge NEXAFS spectra of $Fe(Cp-(CH_3)_5)_2$, Fe(Cp)(Cp−COOH), $Fe(Cp-COOH)_2$, and $Fe(Cp-COCH_3)_2$. The spectra have been offset by a constant for clarity.

4. Calculations

4.1. Fe 2p EHMO Calculations. The simulated Fe 2p edge NEXAFS spectra of $Fe(Cp)_2$, $Fe(Cp-(CH_3)_5)_2$, $Fe(Cp)(Cp-CH_3)$, Fe(Cp)(Cp−Br), Fe(Cp)(Cp−COOH), and $Fe(Cp)(Cp-CH{=}CH_2)$, provided by EHMO simulations are presented in Figure 4a. Detailed peak assignments are provided in Table 4a. Only one band is represented in these simulations because EHMO does not consider the spin−orbit splitting that leads to the separate $2p_{3/2}$ and $2p_{1/2}$ edges.

The relative intensity of the dominant features (A and C) is correctly reproduced in the EHMO calculation; however, the energy splitting between these features is overestimated, and the intensity of the second feature (C) is underestimated relative to experiment. Difficulties with the feature intensity in EHMO-EICVOM calculations are well-known[53] and have been attributed to inadequacies of the EHMO wave functions. The poor reproduction of the energy splitting is attributed to the limitations of the semiempirical parametrization, which can reasonably be expected to be less effective for core excited states. However, the value of EHMO is its qualitative nature of its results—which is entirely consistent with our experimental results—and not the quality of its quantitative predictions.[66] To address the relative shortcomings of the EHMO calculations, we compare the diagrams of relevant unoccupied molecular orbitals provided by ground state DFT calculations with those provided by EHMO calculations (within the EICVOM approximation[63] to simulate the Fe 2p core excited state). These molecular orbital diagrams are presented in the Supporting Information: Figure S2 for the π^* MOs (LUMO to LUMO+6) in core excited $Fe(Cp)_2$, Fe(Cp)(Cp−CH_3), and Fe(Cp)(Cp−COOH), provided by EHMO calculations, and Figure S3 for the same π^* MOs in ground state $Fe(Cp)_2$, Fe(Cp)(Cp−CH_3), and Fe(Cp)(Cp−COOH), provided by DFT calculations performed with the StoBe program and plotted using Molekel program.[67]

TABLE 3: Transition Energies (eV) and Assignments for the Carbon 1s NEXAFS Spectra (Figure 3) of Ferrocene and Substituted Ferrocene Compounds[a]

label	$Fe(Cp)_2$ [29]	$Fe(Cp-(CH_3)_5)_2$	Fe(Cp)(Cp−COOH)	$Fe(Cp-COOH)_2$	$Fe(Cp-COCH_3)_2$	assignment
A			285.42	285.34	285.27	C1s → **Fe3d$_{xz}$/$\pi^*_{(Cp-COOH)\,(Cp-COCH_3)}$**
						C1s → **Fe3d$_{yz}$/$\pi^*_{(Cp)}$**
A	285.7	285.81				C1s → **Fe3d$_{xz,yz}$/$\pi^*_{(Cp)}$**
B			286.38	286.31		C1s → Fe3d/$\pi^*_{(Cp-COOH)}$
B					286.45	C1s → Fe3d/$\pi^*_{(Cp-COCH_3)}$
						C1s →$_{(CO)}$ $\pi^*_{(C=O)}$
C	287.21	287.14	287.1	≈287.2	287.32	C1s → Fe3d/$\pi^*_{(Cp)}$
E		287.91				C1s $_{(CH_3)}$ → $\sigma^*_{(C-H)}$
D				288.41		C1s $_{(CO)}$ → $\pi^*_{(C=CO)}$
D			288.49		288.52	C1s $_{(CO)}$ → $\pi^*_{(C=CO)}$
						C1s $_{(C-CO)}$ → $\pi^*_{(C=CO)}$
						C1s $_{(CH_3)}$ → $\sigma^*_{(C-H)}$
D′				288.82 sh		C1s $_{(C-CO)}$ → $\pi^*_{(C=CO)}$

[a] Localization of the molecular orbital on the metal or a ligand is indicted by bold script. Transition energy values for $Fe(Cp)_2$ were reproduced from ref 29.

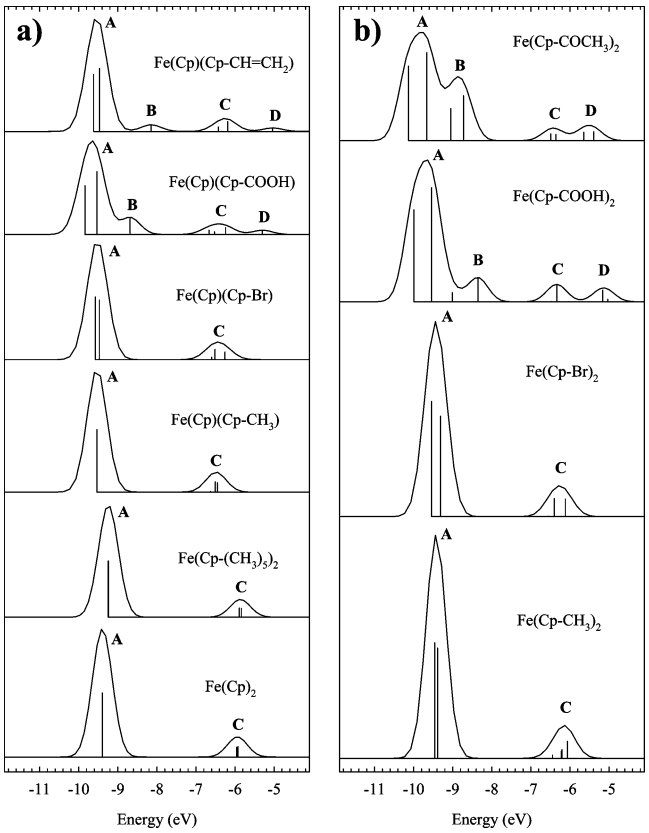

Figure 4. Simulated Fe 2p edge NEXAFS spectra of (a) $Fe(Cp)_2$, $Fe(Cp-(CH_3)_5)_2$, $Fe(Cp)(Cp-CH_3)$, Fe(Cp)(Cp−Br), Fe(Cp)(Cp−COOH), and $Fe(Cp)(Cp-CH=CH_2)$; (b) $Fe(Cp-CH_3)_2$, $Fe(Cp-Br)_2$, $Fe(Cp-COOH)_2$, and $Fe(Cp-COCH_3)_2$ calculated using EHMO theory (CACAO program). The spectra have been offset by a constant for clarity.

The simulated Fe 2p spectrum of $Fe(Cp)_2$ shows two peaks, labeled A and C. The first feature (A) arises from transitions to a pair of degenerate MOs (e_{1g} symmetry) that have a large Fe $3d_{xz}$ and $3d_{yz}$ (the C_5 axis is aligned along the *z*-axis) contribution mixed with Cp π^* character. The second peak (C) arises from transitions to a degenerate Cp π^* MO (e_{2g} symmetry) mixed with a small Fe $3d_{xy}$ and $3d_{x^2-y^2}$ contribution, as indicated by the small AO orbital coefficients.[35] The molecular orbitals for features A and C have similar characters for both the EHMO (core excited) and DFT (ground state) calculations (Figures S2 and S3 in the Supporting Information). In $Fe(Cp)_2$, a set of degenerate MOs exists at slightly lower energy than the molecular orbitals for C; however, these MOs are exclusively ligand (e_{2u}) character with no Fe 3d character and therefore do not contribute to the Fe 2p spectra within the atomic propensity rule (identified in Table 4a as "mute"). These results are similar to that of Hitchcock et al., who used similar EHMO calculations.[28] The similarity of the DFT and EHMO molecular orbitals provides additional support for our use of the EHMO method to simulate the Fe 2p spectra.

The Fe 2p NEXAFS simulations of ferrocene species substituted with a CH_3 or Br group are similar to that of $Fe(Cp)_2$, with a slight lifting of the degeneracy of A and C relative to $Fe(Cp)_2$. The orbital energies of $Fe(Cp-(CH_3)_5)_2$ are slightly reduced compared to those for $Fe(Cp)_2$, especially for feature A. Substitution by a methyl or halogen group has a minor effect on the NEXAFS spectra.

In contrast, the Fe 2p spectrum of Fe(Cp)(Cp−COOH) differs from that of $Fe(Cp)_2$, $Fe(Cp-(CH_3)_5)_2$, Fe(Cp)(Cp−CH_3), and Fe(Cp)(Cp−Br), by the presence of two new features, B and D. Feature A retains a similar character (Fe $3d_{xz}/\pi^*$ MO for the LUMO and Fe $3d_{xy}/\pi^*_{(Cp)}$ for LUMO+1), although the degeneracy of A is lifted due to delocalization of the $3d_{xz}/\pi^*_{(Cp)}$ LUMO onto the substituent (−COOH), which shifts the LUMO toward more negative term values. The LUMO+1 (∼0.30 eV higher) shows no contribution from the substituent and shows a term value similar to that for $Fe(Cp)_2$ (see Supporting Information, Figure S2, for energy correlation diagram and drawing of the individual MOs in the excited state). Feature B (LUMO+2) represents a new feature, where ligand $\pi^*_{(Cp-COOH)}$ character is mixed with a small Fe $3d_{xz}$ contribution. Feature C corresponds to a band of three unoccupied MOs (LUMO+3 through LUMO+5) localized on the Cp ligands with almost no substituent contribution and weak mixing with the Fe metal $3d_{x^2-y^2}$ and $3d_{xy}$ orbitals. This feature is similar to feature C in $Fe(Cp)_2$, but here the degeneracy is lifted. The MO associated to peak D (LUMO+6) has mostly $\pi^*_{(Cp-COOH)}$ character with a small Fe $3d_{x^2-y^2}$ character. The Fe 2p spectrum of Fe(Cp)-(Cp−CH=CH_2) is similar to the spectrum of Fe(Cp)(Cp−COOH).

This increasing complexity in these spectra arises from the presence of strong π^* conjugation between the Cp ring and unsaturated substituents, which lifts the π^* orbital degeneracy and adds spectroscopic features. These ligand−substituent π^* interactions are absent in the alkylated and halogenated ferrocene compounds, so their spectra are similar to those for $Fe(Cp)_2$. A common pattern is observed in the NEXAFS spectra of ferrocene derivatives with substituents containing unsaturations: MOs with π-bonding or nonbonding interactions between the Cp-substituted carbon atom and the substituent appear at lower energy (B), and MOs with π^*-antibonding interactions

TABLE 4: Assignment of EHMO Simulated Fe 2p NEXAFS Spectra (Figure 4)[a]

(a) $Fe(Cp)_2$, $Fe(Cp-(CH_3)_5)_2$, $Fe(Cp)(Cp-CH_3)$, $Fe(Cp)(Cp-Br)$, $Fe(Cp)(Cp-COOH)$, and $Fe(Cp)(Cp-CH=CH_2)$

label	$Fe(Cp)_2$	$Fe(Cp-(CH_3)_5)_2$	$Fe(Cp)(Cp-CH_3)$	$Fe(Cp)(Cp-Br)$	$Fe(Cp)(Cp-COOH)$	$Fe(Cp)(Cp-CH=CH_2)$
A	$Fe3d_{xz}/\pi^*(Cp\ e_{1g})$	$Fe3d_{xz}/\pi^*(Cp\ e_{1g})$	$Fe3d_{xz}/\pi^*(Cp)$	$Fe3d_{yz}/\pi^*(Cp)$	$Fe3d_{xz}/\pi^*(Cp-COOH)^b$	$Fe3d_{xz}/\pi^*(Cp-CH=CH_2)^b$
	$Fe3d_{yz}/\pi^*(Cp\ e_{1g})$	$Fe3d_{yz}/\pi^*(Cp\ e_{1g})$	$Fe3d_{yz}/\pi^*(Cp)$	$Fe3d_{xz}/\pi^*(Cp-Br)^a$	$Fe3d_{yz}/\pi^*(Cp)$	$Fe3d_{yz}/\pi^*(Cp)$
B					$Fe3d_{xz}/\pi^*\mathbf{(Cp-COOH)^n}$	$Fe3d_{xz}/\pi^*\mathbf{(Cp-CH=CH_2)^b}$
mute	$\pi^*(Cp\ e_{2u})$	$\pi^*(Cp\ e_{2u})$	$\pi^*(Cp)$	$\pi^*(Cp)$		
	$\pi^*(Cp\ e_{2u})$	$\pi^*(Cp\ e_{2u})$	$\pi^*(Cp)$			
C	$Fe3d_{xy}/\pi^*\mathbf{(Cp\ e_{2g})}$	$Fe3d_{xy}/\pi^*\mathbf{(Cp\ e_{2g})}$	$Fe3d_{xy}/\pi^*\mathbf{(Cp)}$	$Fe3d_{x^2-y^2}/\pi^*\mathbf{(Cp)}$	$Fe3d_{x^2-y^2}/\pi^*\mathbf{(Cp)}$	$Fed_{x^2-y^2}/\pi^*\mathbf{(Cp)}$
mute						$\pi^*(Cp)$
C	$Fe3d_{x^2-y^2}/\pi^*\mathbf{(Cp\ e_{2g})}$	$Fe3d_{x^2-y^2}/\pi^*\mathbf{(Cp\ e_{2g})}$	$Fe3d_{x^2-y^2}/\pi^*\mathbf{(Cp)}$	$Fe3d_{xy}/\pi^*\mathbf{(Cp)}$	$Fe3d_{xy}/\pi^*\mathbf{(Cp)}$	$Fe3d_{xy}/\pi^*\mathbf{(Cp)}$
				$Fe3d_{x^2-y^2}/\pi^*\mathbf{(Cp-Br)}^a$	$Fe3d_{xy}/\pi^*\mathbf{(Cp)}$	
D					$Fe3d_{x^2-y^2}/\pi^*\mathbf{(Cp-COOH)}^a$	$Fe3d_{x^2-y^2}/\pi^*\mathbf{(Cp-CH=CH_2)}^a$

(b) $Fe(Cp-CH_3)_2$, $Fe(Cp-Br)_2$, $Fe(Cp-COOH)_2$, and $Fe(Cp-COCH_3)_2$

label	$Fe(Cp-CH_3)_2$	$Fe(Cp-Br)_2$	$Fe(Cp-COOH)_2$	$Fe(Cp-COCH_3)_2$
A	$Fe3d_{yz}/\pi^*(Cp)$	$Fe3d_{yz}/\pi^*(Cp)$	$Fe3d_{xz}/\pi^*(Cp-COOH)^b$	$Fe3d_{xz}/\pi^*(Cp-COCH_3)^b$
	$Fe3d_{xz}/^*(Cp)$	$Fe3d_{xz}/\pi^*(Cp-Br)^a$	$Fe3d_{yz}/\pi^*(Cp)$	$Fe3d_{yz}/\pi^*(Cp-COCH_3)^b$
B			$Fe3d_{x^2-y^2}/\pi^*\mathbf{(Cp-COOH)^n}$	$Fe3d_{yz}/\pi^*\mathbf{(Cp-COCH_3)^n}$
			$Fe3d_{yz}/\pi^*\mathbf{(Cp-COOH)^n}$	$Fe3d_{xz}/\pi^*\mathbf{(Cp-COCH_3)^n}$
mute	$\pi^*(Cp)$	$\pi^*(Cp)$	$\pi^*(Cp)$	
C	$Fe3d_{xy}/\pi^*\mathbf{(Cp)}$	$Fe3d_{xy}/\pi^*\mathbf{(Cp)}$	$Fe3d_{xy}/\pi^*\mathbf{(Cp)}$	$Fe3d_{x^2-y^2}/\pi^*\mathbf{(Cp)}$
mute		$\pi^*(Cp-Br)^a$		
C	$Fe3d_{xy}/\pi^*\mathbf{(Cp)}$	$Fe3d_{x^2}\pi^*_{z^2}/\pi^*\mathbf{(Cp)}$		$Fe3d_{xy}/\pi^*\mathbf{(Cp)}$
	$Fe3d_{x^2-z^2}/\pi^*\mathbf{(Cp)}$			
D			$Fe3d_{x^2-y^2}/\pi^*\mathbf{(Cp-COOH)}^a$	$Fe3d_{x^2-y^2}/\pi^*\mathbf{(Cp-COCH_3)}^a$
			$Fe3d_{xz}/\pi^*\mathbf{(Cp-COOH)}^a$	$Fe3d_{xy}/\pi^*\mathbf{(Cp-COCH_3)}^a$

[a] Superscripts indicate the nature of the interactions between Cp substituted carbon and substituent: [b] bonding, [n] nonbonding, and [a] antibonding. Localization of the molecular orbital on the metal or a ligand is indicted by bold script.

(e.g., a node between the Cp and the substitutent) occur at higher energy (D). This pattern is revealed in the MO diagrams, provided in the Supporting Information (Figures S2 and S3). Again, the ground state DFT calculations provide molecular orbital diagrams simlar to those from the Fe 2p EHMO calculations.

The simulated Fe 2p edge NEXAFS spectra of disubstituted ferrocene derivatives, $Fe(Cp-CH_3)_2$, $Fe(Cp-Br)_2$, $Fe(Cp-COOH)_2$, and $Fe(Cp-COCH_3)_2$, are presented in Figure 4b. Detailed peak assignments are provided in Table 4b. The Fe 2p spectra of the disubstituted species are similar to those for the monosubstituted compounds. The substitution in both Cp rings enhances the energy splitting between the MOs associated with features A and C. These features have similar origins as for the comparable monosubstituted ferrocene derivatives (e.g., Feature A: Fe $3d_{xz}/\pi^*_{(Cp)}$ and Fe $3d_{yz}/\pi^*_{(Cp)}$; Feature C: Fe $3d_{xy}/\pi^*_{(Cp)}$ and Fe $3d_{x^2-y^2}/\pi^*_{(Cp)}$, respectively).

In the Fe 2p simulations of $Fe(Cp-COOH)_2$ and $Fe(Cp-COCH_3)_2$, π^* delocalization between the Cp ligand and the substituent leads to additional features B and D. A similar pattern of nonbonding (feature B) and antibonding (feature D) interactions between the Cp ring and substituent is revealed from the MO diagrams.

These EHMO calculations effectively simulate the π^*-conjugation effects in the Fe 2p NEXAFS spectra of substituted ferrocene compounds. These EHMO results are further validated by ground state DFT calculations.

4.2. Carbon 1s DFT Calculations. The C 1s edge NEXAFS spectra of $Fe(Cp)_2$, $Fe(Cp-(CH_3)_5)_2$, $Fe(Cp)(Cp-COOH)$, $Fe(Cp-COOH)_2$, and $Fe(Cp-COCH_3)_2$ simulated by the DFT program StoBe are presented in Figure 5. Each spectrum is the sum of the individual spectra obtained for each carbon atom in the molecules. The detailed spectra for $Fe(Cp-(CH_3)_5)_2$, $Fe(Cp)(Cp-COOH)$, $Fe(Cp-COOH)_2$, and $Fe(Cp-COCH_3)_2$ are available in Supporting Information (Figures S4−S7). Detailed peak assignments are presented in Table 5a,b.

The simulated C 1s spectrum of $Fe(Cp)_2$ is similar to its experimental spectrum, dominated by two peaks, labeled A and C. The lowest energy peak A is associated with a transition to degenerate MOs (e_{1g} character) formed by the overlap of ligand π^* orbitals mixed with Fe $3d_{xz}$ (LUMO) or $3d_{yz}$ (LUMO+1) atomic orbitals. The second strong feature (C) corresponds to π^* orbital that is strongly localized on the Cp ring containing the excited carbon atom. The character of the orbitals associated with these features is similar to that observed in the Fe 2p EHMO calculations; the intensity inversion of the spectral features is consistent with the increased orbital density on iron (band A, A) or on the Cp ring (band C, C), as probed at the Fe 2p edge (A stronger) or the C 1s edge (C stronger). Molecular drawings of LUMO to LUMO+6 for ferrocene, along with $Fe(Cp)(Cp-CH_3)$ and $Fe(Cp)(Cp-COOH)$, in the ground state calculated using StoBe program and plotted using Molekel program[67] are provided in Supporting Information (see Figure S3). The assignment of the $Fe(Cp-(CH_3)_5)_2$ spectrum is similar to that for $Fe(Cp)_2$ for peaks A and C with addition of feature E that originates from methyl carbon atoms.

The C 1s spectrum of $Fe(Cp)(Cp-COOH)$ shows additional features, B and D. Feature A has an origin similar to that in $Fe(Cp)_2$, with a slight lifting of degeneracy from the contribution of the substituent COOH π^*-orbital to the LUMO. The second peak (B) is assigned to an MO formed by the mixture of Fe 3d character mixed with the ligand $\pi^*_{(Cp-COOH)}$ orbital. As in $Fe(Cp)_2$, the third peak (C) is strongly localized to the Cp ring with the C 1s core hole, with little delocalization onto the carbonyl substituent. Feature D is the overlap of the C 1s $\rightarrow \pi^*_{(C=O)}$ transition of the carbonyl group, and D′ is the C_{sub} 1s $\rightarrow \pi^*_{(C=COOH)}$ transition from the chemically shifted substituted Cp ring site (C_{sub}) (see Figure S3 of the Supporting Information for MO drawings from DFT calculations) of $Fe(Cp)(Cp-COOH)$ in ground sate). Similar substituent shifted transitions are observed in functionalized benzene groups, e.g., C 1s(C−

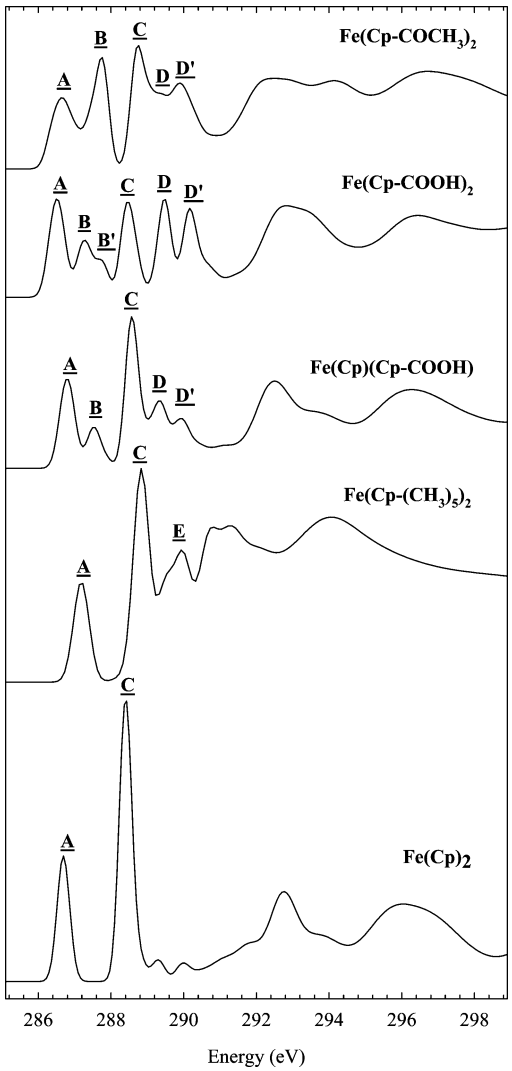

Figure 5. Simulated C 1s NEXAFS spectra of $Fe(Cp)_2$, $Fe(Cp-(CH_3)_5)_2$, Fe(Cp)(Cp−COOH), $Fe(Cp-COOH)_2$, and $Fe(Cp-COCH_3)_2$ calculated using DFT theory (StoBe program). The spectra have been offset by a constant for clarity.

R) → $\pi^*_{(C=C)}$ transition.[68] This splitting is not resolved in the experimental spectrum.

The simulated spectrum of disubstituted $Fe(Cp-COOH)_2$ resembles that of monosubstituted Fe(Cp)(Cp−COOH), with slight variations in peak intensity. A shoulder B′ arises from transitions from carbon atoms next to C_{sub} to a mixed orbital between the two Cp−COOH ligands; however, this feature is not resolved in the experimental C 1s spectra (see Supporting Information, Figure S5). The intensity of features D and D′ increase with the number of carbonyl and substituted Cp carbon atoms in the disubstituted $Fe(Cp-COOH)_2$ molecule; this splitting is resolved in the experimental spectrum.

The simulated C 1s NEXAFS spectrum of disubstituted $Fe(Cp-COCH_3)_2$ differs from $Fe(Cp-COOH)_2$ in the lack of splitting in feature B and the decreased relative intensity of feature A. Feature B in $Fe(Cp-COCH_3)_2$ is dominated by the strong C 1s → $\pi^*_{(C=O)}$ transition, which appears at lower energy in this ketone substituent relative to the carboxylic acid substituent.[69] This carbonyl contribution increases the intensity of B, which now is more intense than A in the simulation and experiment. Feature D in $Fe(Cp-COCH_3)_2$ is assigned to C_{sub} 1s → $\pi^*_{(C=COCH_3)}$ transition and feature D′ to $C_{(CH_3)}$ 1s → $\sigma^*_{(C-H)}$ transition.

The presence, intensity and evolution of features B, D, and D′ are well reproduced in the DFT simulations of the C 1s spectrum of the substituted ferrocene species. These features arise from the stoichiometrically weighted C 1s contribution of the substituent groups (e.g., COOH, $COCH_3$, or CH_3) to the spectra, as well as π^* interactions between the Cp rings and the substituents containing unsaturation. These π^* conjugation interactions provide definitive evidence for the strong role of a covalent bonding model in the NEXAFS spectra of closed shelled ferrocene derivatives (see ref 35 for a comprehensive discussion).

5. Discussion

5.1. Fe 2p Edge. The importance of covalent hybridization between metal 3d orbitals and ligand π^* orbitals in the interpretation of NEXAFS spectroscopy of transition metal complexes has been indicated in several studies.[20,35−39,46,70] In the investigation of planar Ni $3d^8$ and Cu $3d^9$,[10] low-spin complexes, the presence of an intense band at the L_2 and L_3 edges was assigned to metal-to-metal transition (2p → 3d), followed by satellites peaks at a few eV higher energy.[36−39] These satellites' features were assigned as a transition to a molecular orbital showing strong metal-covalent character, and identified as a metal-to-ligand charge-transfer (MLCT) transition (2p → $3d_{metal}/\pi^*_{ligand}$). These assignments were supported by Hartree−Fock-based static exchange approximation and DFT calculations.[37] In the study of $K_2Ni(CN)_4 \cdot H_2O$, Ni(dimethylglyoximato)$_2$, and $[(n\text{-}C_4H_9)_4N]_2$ [Ni(maleonitriledithiolato)$_2$] complexes the intensities of the MLCT transition were observed to vary as $K_2Ni(CN)_4 \cdot H_2O$ > Ni(dimethylglyoximato)$_2$ > $[(n\text{-}C_4H_9)_4N]_2$ [Ni(maleonitriledithiolato)$_2$].[39] The authors indicated that the $3d_{metal}/\pi^*_{ligand}$ valence MO was formed by occupied metal orbital mixed with unoccupied ligand π^*-orbital, corresponding to a metal to ligand back-donation MO. The decrease in MLCT transitions intensity was then found consistent with the reduction in the back-donation strength among these three complexes, supporting strongly the importance of covalency in the NEXAFS spectra of these species.[38,39] A separate study on ferrocene and ferrocenium hexafluorophosphate showed that the use of covalent bonding model was more efficient than multiplet model in the interpretation of closed shelled metallocenes spectra.[35] In this study, we show that electron donating/withdrawing properties of the ligands and substitutents, as well as conjugation between the Cp and substituent π^* character significantly affect the energy and intensity of Fe 2p NEXAFS transitions.

Fe 2p NEXAFS spectra of substituted ferrocene compounds resemble that of ferrocene by the presence of intense feature labeled A followed at higher energy by weaker peak, C. Feature A is assigned to transitions to MOs with large Fe $3d_{xz}$ and Fe $3d_{yz}$ character, mixed with small ligand $\pi^*_{(Cp)}$ contribution, or metal-to-metal transition, and feature C was assigned to $\pi^*_{(Cp)}$ MOs mixed with some Fe $3d_{xy}$ and Fe $3d_{x^2-y^2}$ contribution, corresponding to a metal-to-ligand charge-transfer transition (MLCT).[35] Moreover, in the ground state the metal $3d_{xy}$ and $3d_{x^2-y^2}$ orbitals are occupied and ligand $\pi^*_{(Cp)}$ orbitals are unoccupied; therefore, feature C is associated with a back-donation (metal-to-ligand) MO. As evident in Figure 2, the nature of feature C is relatively similar in the set of substituted ferrocene compounds. This is in contrast to the study of nickel complexes by Hatsui et al., where a strong relationship between the strength of back-donation and the intensity of feature C was observed.[39] In substituted ferrocene molecules, we assume that the substituent on the Cp ring has only a weak effect on the back-donation between the Cp ring ligand and the iron atom.

TABLE 5: Assignment of DFT Simulated C1s NEXAFS Spectra (Figure 5)

(a) $Fe(Cp)_2$ and $Fe(Cp-(CH_3)_5)_2$

	$Fe(Cp)_2$		**$Fe(Cp-(CH_3)_5)_2$**	
feature	core hole location	optical orbital	core hole location	optical orbital
A	Cp carbons	$Fe3d_{xz}/e_{1g}$ $Fe3d_{yz}/e_{1g}$	Cp carbons	$Fe3d_{xz}/ e_{1g}$-like $Fe3d_{yz}/e_{1g}$-like
C	Cp carbons	$Fe3d_{x^2-y^2}/e_2''$ (only Cp with excited carbon)	Cp carbons	$Fe3d_{x^2-y^2}/e_2''$-like (only Cp with excited carbon)
E			methyl carbons	$\sigma^*_{(C-H)}$

(b) $Fe(Cp)(Cp-COOH)$, $Fe(Cp-COOH)_2$, and $Fe(Cp-COCH_3)_2$

	$Fe(Cp)(Cp-COOH)$		**$Fe(Cp-COOH)_2$**		**$Fe(Cp-COCH_3)_2$**	
feature	core hole location	optical orbital	core hole location	optical orbital	core hole location	optical orbital
A	C_{sub}, C2−C5, C1′−C5′	$Fe3d_{xz}/\pi^*_{(C=COOH)}$ $Fe3d_{yz}/\pi^*_{(Cp)}$	C_{sub}, C_{sub}' C2−C5, C2′−C5′	$Fe3d_{xz}/\pi^*_{(C=COOH)}$ $Fe3d_{yz}/\pi^*_{(Cp)}$	C_{sub}, C_{sub}' C2−C5, C2′−C5′	$Fe3d_{xz}/\pi^*_{(Cp-COCH_3)}$ $Fe3d_{yz}/\pi^*_{(Cp-COCH_3)}$
B	C2−C5	$Fe3d_{x^2-y^2}/\pi^*_{(Cp-COOH)}$	C2−C5, C2′−C5′	$Fe3d_{x^2-y^2}/\pi^*_{(Cp-COOH))}$	C3−C5, C3′−C5′	$Fe3d/\pi^*_{(Cp-COCH_3)}$
					$C_{=O}$, $C_{=O}'$	$Fe3d/\pi^*_{(C=O)}$
B′			C2, C5, C2′, C5′	$Fe3d_{z^2}/\pi^*_{(Cp-COOH))}$		
C	C2−C5 C1′−C5′	$Fe3d_{x^2-y^2}/e''_2$-like	C2−C5, C2′−C5′	$Fe3d_{x^2-y^2}/\pi^*_{(Cp)}$	C2−C5, C2′−C5′	$Fe3d_{x^2-y^2}/\pi^*_{(Cp)}$
D	$C_{=O}$	$Fe3d_{xy}/\pi^*_{(C=COOH)}$	$C_{=O}$, $C_{=O}'$	$Fe3d_{xy}/\pi^*_{(C=COOH)}$	C_{sub}, C_{sub}'	$Fe3d/\pi^*_{(C=COCH_3)}$
D′	C_{sub}	$Fe3d_{xy}/\pi^*_{(C=COOH)}$	C_{sub}, C_{sub}'	$Fe3d_{xy}/\pi^*_{(C=COOH)}$	C2, C5, C2′, C5′	$Fe3d/\pi^*_{(C=COCH_3)}$
					C_{methyl}, C_{methyl}'	$\sigma^*_{(C-H)}$

The effect of the electronegativity of the ligands can also be considered. Electron withdrawing groups around the metal center will deplete the electron density on the metal atom and increase electron−nuclear Coulombic attraction,[15] leading to an increased Fe 2p ionization potential (IP) and a shift toward high energy of the transition. Increase in electron−nuclear Coulombic attraction affects as well the energy of the valence orbitals leading to an augmentation of the term values and a shift toward low energy of the transition. The Fe 2p spectrum of $Fe(Cp-(CH_3)_5)_2$ is similar to the gas-phase spectrum of ferrocene (ISEELS) recorded by Hitchcock et al.[28,29] The Fe 2p ionization potential of $Fe(Cp-(CH_3)_5)_2$ is expected to be 1 eV lower energy than for ferrocene, as the methyl groups are electron donating.[71] This ionization potential shift is partially compensated by an opposite shift in the valence e_{1g} orbital (feature A) to higher energy. The net effect is a slight shift of feature A to lower energy in the Fe 2p NEXAFS spectrum of $Fe(Cp-(CH_3)_5)_2$ relative to $Fe(Cp)_2$ (NB feature energy = ionization potential + orbital energy). This compensating shift in the IP and the valence orbital energy is common in NEXAFS spectroscopy.[69] The energy difference between comparable features in $Fe(Cp)_2$ and $Fe(Cp-(CH_3)_5)_2$ is smaller for feature A ($\Delta = 0.03$ eV) than for feature C ($\Delta = 0.32$ eV) (see Table 2). This suggests that the energy of the unoccupied orbitals localized on the metal atom is more affected by the variations in electron−nuclear Coulombic attraction than ligand localized MOs. In the case of Fe(Cp)(Cp−COOH) and $Fe(Cp-COOH)_2$, the carboxylic acid group is electron withdrawing, and the ionization potential should increase, yet a shift toward low energy is observed for features A and C compared to the case for $Fe(Cp)_2$. As indicated by EHMO calculations, delocalization of the Fe $3d/\pi^*_{(Cp)}$ LUMO onto the substituent (−COOH) shifts the LUMO toward more negative term values. Combined effects of increased electron−nuclear Coulombic attraction and substituent (−COOH) stabilization effect compensate for the increase in ionization potential. The acetyl group ($COCH_3$) is a weaker electron withdrawing group than carboxylic acid yet larger stabilization effect of the substituent ($-COCH_3$), as indicated by EHMO calculations, shifts feature A further to lower energy.

In the studies performed by Hitchcock et al. on manganese, iron, and cobalt complexes using carbonyl and cyclopentadienyl as ligands, the authors reported that the spectra of alkane or alkene substitued ferrocene complexes were similar and that the presence of unsaturation in the substituent had little effect on Fe 2p spectra.[29] In their investigation of ferrocene-labeled peptides and carboxylic acid substituted ferrocene complexes, Wilks et al. find that their Fe 2p spectra are unaffected by the substituent type.[18] In contrast, here we find that there is a significant dependence of the identity and the number of substituents present on the Cp ring. We also re-assign feature C to Cp π^* (e_{2g}) MO, which had been formerly assigned by Wen et al.[29] to transition to Cp π^* (e_{2u}) and by Wilks et al.[18] to transition to a C−H σ^* core excited state. The MO corresponding to peak C is incorrectly labeled by Hitchcock et al. as e_{2u} symmetry. As the 3d orbitals in the D_{5d} point group transform as A_{1g}, E_{1g}, and E_{2g}, an MO formed from the mixture of metal 3d orbitals and the Cp π^* MOs cannot have e_{2u} symmetry.

A key observation from this work is the presence of new features B and D in the Fe 2p spectra of ferrocene derivatives with substituents containing unsaturations. Our EHMO calculations reveal that these features arise from strong π^* conjugation between the Cp ring and the substituent groups, where bonding or nonbonding interactions are observed at lower energy (feature B) and antibonding interactions are observed at higher energy (feature D). The Fe 2p spectrum of ferrocene derivates with saturated substituents remains similar to that of ferrocene.

In the gas-phase ISEELS spectrum of $Fe(Cp)(Cp-CH{=}CH_2)$ recorded by Wen et al., the additional features we label as B and D are not resolved.[29] The EHMO calculations presented here indicate that these features are relatively weak. We suggest

that such weak peaks could not be resolved in the relatively low-energy resolution ISEELS spectra of Fe(Cp)(Cp−CH═CH_2) of Wen et al.[29]

5.2. C 1s Edge. The C 1s NEXAFS spectrum of Fe(Cp−$(CH_3)_5)_2$ is similar to that of $Fe(Cp)_2$. Feature A is assigned to transition to Fe $3d_{xz,yz}$ orbitals, with a small ligand component. Feature C is assigned to transition to localized cyclopentadiene π^* orbital. Additional features are observed in the C 1s NEXAFS spectra of Fe(Cp)(Cp−COOH), $Fe(Cp-COOH)_2$, and $Fe(Cp-COCH_3)_2$, depending on the number and type of substituent. DFT calculations and spectral comparisons indicate that the spectroscopic contribution of the substituent carbon atoms (e.g., CH_3, COOH, $COOCH_3$) as well as π^*-conjugation between the Cp ring and the substituents are responsible for these additional features.

In an ISEELS spectroscopy study of alkane and alkene substituted ferrocene molecules, similar C1s spectra were reported for ferrocene and substituted ferrocene compounds, suggesting that substituents have little influence on the electronic structure of the metallocene.[29] Our assignment of the C 1s spectrum of $Fe(Cp-(CH_3)_5)_2$ is consistent with this conclusion. However, our higher energy resolution data show that there is a significant substituent effect on the spectral shape of Fe(Cp)-(Cp−COOH), $Fe(Cp-COOH)_2$, and $Fe(Cp-COCH_3)_2$. Our DFT calculations and a comparison to the Fe 2p spectra show that this effect arises from π^* conjugation and the spectral contribution of the substituent. Our findings at the C1s edge are consistent with the results obtained by Wilks et al. in their study on ferrocene-labeled peptides.[18]

6. Conclusion

Our study of ferrocene and substituted-ferrocene compounds by NEXAFS spectroscopy demonstrates that the identity of the substitutents on the Cp ring can play a considerable role in the spectral shape of Fe 2p and C 1s NEXAFS spectra. The NEXAFS spectra are affected by the electron withdrawing/donating properties of the substitutents as well as π^*-conjugation between unsaturated substitutents and the Cp ring. Saturated substitutents only have a minor effect on the NEXAFS spectra of functionalized ferrocene molecules. Our findings are supported by EHMO and DFT calculations.

Acknowledgment. This work is supported by Natural Sciences and Engineering Research Council, the Canadian Foundation for Innovation, the Canada Research Chair program, and the University of Saskatchewan. Spectroscopy measurements were performed at the Canadian Light Source, which is supported by NSERC, NRC, CIHR, and the University of Saskatchewan.

Supporting Information Available: Discussion and illustration of carbon 1s NEXAFS spectra normalization. Molecular orbitals diagrams and energy correlation diagrams for Fc(Cp), Fe(Cp) (Cp−Me) and Fe(Cp) (Cp-COOH) calculated by EHMO and DFT calculations. DFT simulation of the C 1s NEXAFS spectra of $Fe(Cp-Me_5)_2$, Fe(Cp) (Cp−COOH), $Fe(Cp-COOH)_2$ and $Fe(Cp-COCH_3)_2$. This material is available free of charge via the Internet at http://pubs.acs.org.

References and Notes

(1) Van Staveren, D. R.; Metzler-Nolte, N. *Chem. Rev.* **2004**, *104*, 5931.
(2) Kraatz, H. B. *J. Inorg. Organomet. Polym. Mater.* **2005**, *15*, 83.
(3) Chen, D.; Li, J. *Surf. Sci. Rep.* **2006**, *61*, 445.
(4) Horie, M.; Sakano, T.; Osakada, K. *J. Organomet. Chem.* **2006**, *691*, 5935.
(5) Lambert, C.; Kriegisch, V.; Terfort, A.; Zeysing, B. *J. Electroanal. Chem.* **2006**, *590*, 32.
(6) Zheng, F.; Perez-Dieste, V.; McChesney, J. L.; Luk, Y.-Y.; Abbott, N. L.; Himpsel, F. J. *Surf. Sci.* **2005**, *587*, L191.
(7) Manners, I. *Synthetic Metal-Containing Polymers*; WILEY-VCH: Weinheim, 2004.
(8) Manners, I. *Science* **2001**, *294*, 1664.
(9) Abd-El-Aziz, A. S.; Manners, I. *J. Inorg. Organomet. Polym. and Materials* **2005**, *15*, 157.
(10) Hudson, R. D. A. *J. Organomet. Chem.* **2001**, *637*−*639*, 47.
(11) Paquet, C.; Cyr, P. W.; Kumacheva, E.; Manners, I. *Chem. Commun.* **2004**, 234.
(12) Manners, I. *J. Opt. A: Pure Appl. Opt.* **2002**, *4*, S221.
(13) Kulbaba, K.; Manners, I. *Macromol. Rapid Commun.* **2001**, *22*, 711.
(14) Neuse, E. W. *J. Inorg. Organomet. Polym. Mater.* **2005**, *15*, 3.
(15) Stohr, J. *NEXAFS Spectroscopy*; Springer-Verlag: Berlin, 1996.
(16) Ade, D. H.; Urquhart, S. G. X-ray Spectromicroscopy of Polymers. In *Chemical Applications of Synchrotron Radiation*; Sham, T.-K., Ed.; World Scientific: Singapore 2002.
(17) Moewes, A.; MacNaughton, J.; Wilks, R.; Lee, J. S.; Wettig, S. D.; Kraatz, H. B.; Kurmaev, E. Z. *J. Electron Spectrosc. Relat. Phenom.* **2004**, *137*−*140*, 817.
(18) Wilks, R. G.; MacNaughton, J. B.; Kraatz, H. B.; Regier, T.; Moewes, A. *J. Phys. Chem. B* **2006**, *110*, 5955.
(19) Balasubramanian, M.; Giacomini, M. T.; Lee, H. S.; McBreen, J.; Sukamto, J. H. *J. Electrochem. Soc.* **2002**, *149*, D137.
(20) Wasinger, E. C.; De Groot, F. M. F.; Hedman, B.; Hodgson, K. O.; Solomon, E. I. *J. Am. Chem. Soc.* **2003**, *125*, 12894.
(21) Abd-El-Aziz, A. S.; Todd, E. K.; Ma, G. Z. *J. Polym. Sci., Pt. A: Polym. Chem.* **2001**, *39*, 1216.
(22) Abd-El-Aziz, A. S.; Todd, E. K. *Coord. Chem. Rev.* **2003**, *246*, 3.
(23) Kealy, T. J.; Pauson, P. L. *Nature* **1951**, *168*, 1039.
(24) Wilkinson, G.; Rosenblum, M.; Whiting, M. C.; Woodward, R. B. *J. Am. Chem. Soc.* **1952**, *74*, 2125.
(25) Dunitz, J. D.; Orgel, L. E.; Rich, A. *Acta Crystallogr.* **1956**, *9*, 373.
(26) Iwai, K.; Iwai, M.; Suto, K.; Nakashima, S.; Motoyama, I.; Sano, H.; Ikemoto, I.; Kosugi, N.; Kuroda, H. *Bull. Chem. Soc. Jpn.* **1986**, *59*, 2675.
(27) Ruiz-Lopez, M. F.; Loos, M.; Goulon, J.; Benfatto, M.; Natoli, C. R. *Chem. Phys.* **1988**, *121*, 419.
(28) Hitchcock, A. P.; Wen, A. T.; Ruhl, E. *Chem. Phys.* **1990**, *147*, 51.
(29) Wen, A. T.; Ruhl, E.; Hitchcock, A. P. *Organometallics* **1992**, *11*, 2559.
(30) Fronzoni, G.; Decleva, P.; Lisini, A.; Ohno, M. *J. Electron Spectrosc. Relat. Phenom.* **1993**, *62*, 245.
(31) Ruhl, E.; Hitchcock, A. P. *J. Am. Chem. Soc.* **1989**, *111*, 5069.
(32) De Groot, F. *Coord. Chem. Rev.* **2005**, *249*, 31.
(33) Van der Laan, G.; Zaanen, J.; Sawatzky, G. A.; Karnatak, R.; Esteva, J.-M. *Phys. Rev. B* **1986**, *33*, 4253.
(34) Solomon, E. I.; Hedman, B.; Hodgson, K. O.; Dey, A.; Szilagyi, R. K. *Coord. Chem. Rev.* **2005**, *249*, 97.
(35) Otero, E.; Urquhart, S. G. Manuscript in preparation.
(36) Hatsui, T.; Takata, Y.; Kosugi, N. *Chem. Phys. Lett.* **1998**, *284*, 320.
(37) Petterson, L. G. M.; Hatsui, T.; Kosugi, N. *Chem. Phys. Lett.* **1999**, *311*, 299.
(38) Takata, Y.; Hatsui, T.; Kosugi, N.; Agui, A.; Magnuson, M.; Sathe, C.; Rubensson, J.-E.; Nordgren, J. *J. Electron Spectrosc. Relat. Phenom.* **2001**, *114*−*116*, 909.
(39) Hatsui, T.; Kosugi, N. *J. Electron Spectrosc. Relat. Phenom.* **2004**, *136*, 67.
(40) Ruhl, E.; Wen, A. T.; Hitchcock, A. P. *J. Electron Spectrosc. Relat. Phenom.* **1991**, *57*, 137.
(41) Regier, T.; Paulsen, J.; Wright, G.; Coulthard, I.; Tan, K.; Sham, T. K.; Blyth, R. I. R. "Commissioning of the Spherical Grating Monochromator Soft X-ray Spectroscopy Beamline at the Canadian Light Source"; Synchrotron Radiation Instrumentation: Ninth International Conference on Synchrotron Radiation Instrumentation, 2006, Daegu, Korea.
(42) Peng, G.; Van, Elp, J.; Jang, H.; Que, L.; Armstrong, W. H.; Cramer, S. P. *J. Am. Chem. Soc.* **1995**, *117*, 2515.
(43) Wang, H.; Peng, G.; Miller, L. M.; Scheuring, E. M.; George, S. J.; Chance, M. R.; Cramer, S. P. *J. Am. Chem. Soc.* **1997**, *119*, 4921.
(44) Collison, D.; Garner, D. C.; McGrath, C. M.; Mosselmans, J. F. W.; Roper, M. D.; Seddon, J. M. W.; Sinn, E.; Young, N. A. *J. Synchrotron Radiation* **1999**, *6*, 585.
(45) Vinogradov, A. S.; Preobrajenski, A. B.; Krasnikov, S. A.; Chasse, T.; Szargan, R.; Knop-Gericke, A.; Schlogl, R.; Bressler, P. *Surf. Rev. Lett.* **2002**, *9*, 359.
(46) Hocking, R. K.; Wasinger, E. C.; De Groot, F. M. F.; Hodgson, K. O.; Hedman, B.; Solomon, E. I. *J. Am. Chem. Soc.* **2006**, *128*, 10442.

(47) Crocombette, J. P.; Pollak, M.; Jollet, F.; Thromat, N.; Gautier-Soyer, M. *Phys. Rev. B* **1995**, *52*, 3143.
(48) Francis, J. T.; Turci, C. C.; Tyliszczak, T.; De Souza, G. G. B.; Kosugi, N.; Hitchcock, A. P. *Phys. Rev. A* **1995**, *52*, 4665.
(49) Urquhart, S. G.; Hitchcock, A. P.; Priester, R. D.; Rightor, E. G. *J. Polym. Sci., PartPt.B: Polym. Phys.* **1995**, *33*, 1603.
(50) Mealli, C.; Proserpio, D. M. *J. Chem. Educ.* **1990**, *67*, 399.
(51) Hitchcock, A. P.; Urquhart, S. G.; Rightor, E. G. *J. Phys. Chem.* **1992**, *96*, 8736.
(52) Hitchcock, A. P.; Urquhart, S. G.; Wen, A. T.; Kilcoyne, A. L. D.; Tyliszczak, T.; Ruhl, E.; Kosugi, N.; Bozek, J. D.; Spencer, J. T.; McIlroy, D. N.; Dowben, P. A. *J. Phys. Chem. B* **1997**, *101*, 3483.
(53) Urquhart, S. G.; Hitchcock, A. P.; Smith, A. P.; Ade, H.; Rightor, E. G. *J. Phys. Chem. B* **1997**, *101*, 2267.
(54) Brock, C. P.; Fu, Y. *Acta Crystallogr. Sect. B-Struct. Sci.* **1997**, *53*, 928.
(55) Arrais, A.; Diana, E.; Gobetto, R.; Milanesio, M.; Viterbo, D.; Stanghellini, P. L. *Eur. J. Inorg. Chem.* **2003**, 1186.
(56) Lin, L.; Berces, A.; Kraatz, H. B. *J. Organomet. Chem.* **1998**, *556*, 11.
(57) Braga, D.; Polito, M.; D'Addario, D. *Cryst. Growth Des.* **2004**, *4*, 1109.
(58) Palenik, G. J. *Inorg. Chem.* **1970**, *9*, 2424.
(59) Foucher, D. A.; Honeyman, C. H.; Lough, A. J.; Manners, I.; Nelson, J. M. *Acta Crystallogr. Sect. C-Cryst. Struct. Commun.* **1995**, *C51*, 1795.
(60) Hnetinka, C. A.; Hunter, A. D.; Zeller, M.; Lesley, G. M. J. *Acta Crystallogr. Sect. E-Struct. Rep. Online* **2004**, *E60*, m1806.
(61) Dong, T.-Y.; Hwang, M.-Y.; Hsu, T.-L.; Schei, C.-C.; Yeh, S.-K. *Inorg. Chem.* **1990**, *29*, 80.
(62) Dong, T.-Y.; Hendrickson, D. N.; Iwai, K.; Cohn, M. J.; Geib, S. J.; Rheingold, A. L.; Sano, H.; Motoyama, I.; Nakashima, S. *J. Am. Chem. Soc.* **1985**, *107*, 7996.
(63) Schwarz, W. H. E. *Chem. Phys.* **1975**, *11*, 217.
(64) Huo, B.; Hitchcock, A. P. Simile2 Software, 1996.
(65) Hermann, K.; Petterson, L. G. M.; Casida, M. E.; Daul, C.; Goursot, A.; Koester, A.; Proynov, E.; St-Amant, A.; Salahub, D. R.; Contributing authors: Carravetta, V.; Duarte, H.; Friedrich, C.; Godbout, N.; Guan, J.; Jamorski, C.; Leboeuf, M.; Leetmaa, M.; Nyberg, M.; Pedocchi, L.; Sim, F.; Triguero, L.; Vela, A. StoBe Software, StoBe-DeMon Version 2.1, 2005.
(66) Gimarc, B. M. *Molecular Structure and Bonding*; Academic Press: New York, 1979.
(67) Portmann, S.; Fluekiger, P. F. MOLEKEL; 4.3.win32 ed.; Swiss-National-Supercomputing-Centre: Geneva, 2002.
(68) Cooney, R. R.; Urquhart, S. G. *J. Phys. Chem. B* **2004**, *108*, 18185.
(69) Urquhart, S. G.; Ade, H. *J. Phys. Chem.* **2002**, *106*, 8531.
(70) Hocking, R. K.; Wasinger, E. C.; Yan, Y.-L.; De Groot, F. M. F.; Walker, F. A.; Hodgson, K. O.; Hedman, B.; Solomon, E. I. *J. Am. Chem. Soc.* **2007**, *129*, 113.
(71) Gassman, P. G.; Deck, P. A. *Organometallics* **1994**, *13*, 2890.